Pattern formation in interface depinning and other models: Erratically moving spatial structures

Supriya Krishnamurthy and Mustansir Barma
Theoretical Physics Group, Tata Institute of Fundamental Research, Homi Bhabha Road, Mumbai 400 005, India
(Received 16 September 1997)

We study erratically moving spatial structures that are found in a driven interface in a random medium at the depinning threshold. We introduce a bond-disordered variant of the Sneppen model and study the effect of extremal dynamics on the morphology of the interface. We find evidence for the formation of a structure that moves along with the growth site. The time average of the structure, which is defined with respect to the active spot of growth, defines an activity-centered pattern. Extensive Monte Carlo simulations show that the pattern has a tail that decays slowly, as a power law. To understand this sort of pattern formation, we write down an approximate integral equation involving the local interface dynamics and long-ranged jumps of the growth spot. We clarify the nature of the approximation by considering a model for which the integral equation is exactly derivable from an extended master equation. Improvements to the equation are considered by adding a second coupled equation that provides a self-consistent description. The pattern, which defines a one-point correlation function, is shown to have a strong effect on ordinary space-fixed two-point correlation functions. Finally we present evidence that this sort of pattern formation is not confined to the interface problem, but is generic to situations in which the activity at successive time steps is correlated, such as, for instance, in several other extremal models. We present numerical results for activity-centered patterns in the Bak-Sneppen model of evolution and the Zaitsev model of low-temperature creep. [S1063-651X(98)07903-3]

PACS number(s): 47.54.+r, 68.10.Gw, 05.40.+j, 47.55.Mh

I. INTRODUCTION

Driven interfaces in random media present several features of interest, with regard to both the morphology of the moving interface as well as the dynamics of the growth process. Experiments have been performed on several sorts of systems, ranging from fluid flow in porous media [1–5] to propagation of burning fronts [6]. These indicate that the disorder in the medium affects the properties of the interface in a crucial way. In particular, the large-distance scaling properties differ considerably from those of interfaces in uniform media. In both theoretical and experimental investigations, it is customary to characterize the spatial structure of the interface by its *roughness*. The main point of this paper is to show that there is sometimes an unusual sort of pattern formation [7] in the system, which results in the interface acquiring a *time-averaged shape*. In such situations, this pattern provides an alternative characterization of interface morphology.

A customary measure of the roughness is provided by the exponent α, defined by $W \sim L^{\alpha}$, where W is the root mean squared width of the interface and L is the size of the system. The experiments mentioned above, and others similar to these, report an anomalously large value of α — large compared to the predictions of existing theories for interface growth in nonrandom media [8]. It is recognized that the quenched nature of the disorder in the medium is responsible for this difference in scaling properties of the interface. Unlike thermal noise, which varies rapidly, a portion of the interface subject to a quenched-noise environment continues to experience the same forces until the growth process takes it forward to a new region. The pinning effect of quenched noise has a strong effect on the large scale properties of the interface.

Several theoretical models have been put forward to try to account for the effect of quenched disorder on the properties of the interface; Ref. [9] gives an account of some of the early work and the relationship to other problems involving pinning, while [10] is a recent review. Among various proposals put forward to explain anomalous roughening are theories based on continuum equations with quenched disorder [11–16], the inclusion of noise with power-law amplitude [17,18] or long-ranged correlation [19–21], power-law distributions of pinning-center strengths [22], as well as a class of models with microscopic rules based on directed percolation [5,23,24] and models that relate the large-scale structure to the wetting properties of the invading fluid [26]. A number of these models base the explanation of anomalous roughening on the phenomenon of critical depinning, which is relevant to an interface just at the threshold of motion. In the opposite limit of large velocity, the interface encounters the disorder at any site only for a short time, suggesting that the quenched nature of disorder is not important in this limit, and the interface behaves much as in a nonrandom medium [14]. However, this is not true at low velocities of the interface near the depinning threshold. In particular, the limit of zero velocity is thought to be a dynamical critical point [9] where the scaling properties of the interface are strongly affected by the disorder.

In a certain class of models, the quenched disorder enters as barriers of random strengths that impede interface motion. The formation of infinitely long directed percolating paths of these barriers is of special significance, as such paths can block the entire interface effectively [5,23–25]. The model proposed by Sneppen [24] involves ''extremal'' dynamics: At each time step, the interface advances only along the weakest of the barriers. Extremal models were first introduced much earlier, in the context of invasion percolation for two-phase fluid flow in porous media, with a nonwetting fluid displacing a wetting one [27–29]. The predictions of this invasion percolation model were borne out by experiments [30]. Dynamical correlation functions involving the

 © 1998 The American Physical Society

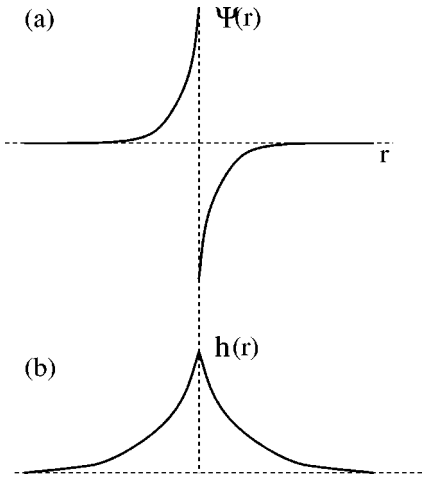

FIG. 1. A schematic picture of the activity-centered pattern in an *untilted* ($m=0$) interface showing (a) the height gradient pattern as defined in Eq. (1), (b) the interface profile obtained by integrating the pattern in (a). The discontinuity at the origin in (a) leads to a cusp at the origin in (b), implying that the active site is most likely at the peak.

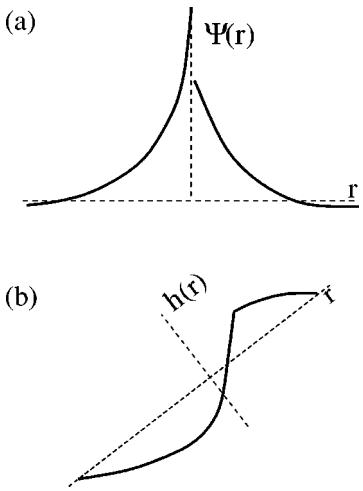

FIG. 2. A schematic picture of the activity-centered pattern in a *tilted* interface ($m\neq 0$), in (a) height gradients (b) the interface profile obtained by integrating the pattern in (a). As can be seen in (b), there is a larger than nominal slope near the active site.

center of activity in invasion percolation obey scaling [31,32], and the process defines a self-organized critical phenomenon [32]; the interface organizes itself to align along critical paths bordered by large barriers, without the necessity of tuning any external parameters. The model proposed by Sneppen [24] is a modification of the invasion percolation model, incorporating surface tension effects that prevent very strong local convolutions of the interface, resulting in a self-affine, rather than self-similar, geometry. An extremal model close to the Sneppen model was shown to result [33] from a model of wetting-fluid invasion, by considering an interface advancing by merging meniscus arcs between adjacent pairs of pinning centers.

An interesting feature of extremal dynamics is that it induces strong spatial correlation in sites at which growth occurs [34–36] at successive time steps. In this paper we introduce and study a variant of the Sneppen model and show that the interface develops an interesting time-averaged structure as a result of correlations. The defining equation for the structure is

$$\Psi(r)\equiv\tfrac{1}{2}[\langle\nabla h(r+R(t))\rangle-m], \tag{1}$$

where $R(t)$ is the position of the active site at time t, $h(r')$ denotes the height at the site r', $\langle\cdots\rangle$ is a time average in the steady state, and m is the overall slope of the interface. The unusual point is that this structure $\Psi(r)$ is not fixed in space, but moves with its center always at the growth site, which itself follows an erratic path. The moving origin is crucial to the definition, as time averages performed at a fixed point in space reveal no structure at all. This average structure defines a pattern, and we study its formation numerically and analytically.

Figure 1(a) depicts schematically the activity-centered pattern in height gradients with respect to the moving origin, for the untilted ($m=0$) interface. As can be seen, the interface develops an overall shape that is described by the height-gradient profile $\Psi(r)$. The tail of the pattern falls slowly at large distances, as a power law. The corresponding height profile of the interface $h(r)$ with respect to the active site is represented in Fig. 1(b). The nature of the pattern is sensitive to tilt, and Fig. 2 shows the height-gradient pattern and height profile for a tilted interface.

We propose that this pattern is a simple way of characterizing a new aspect of the morphology of the interface. Traditional ways of characterizing the morphology involve, as has already been mentioned, determining the roughness exponent α. However, such a definition does not hone in on the overall *shape* of the interface. In situations such as the one considered in this paper when the interface does develop a nontrivial structure, the pattern is a useful quantitative characterization. An important point about the time-averaged pattern is that Eq. (1) defines a one-point correlation function. As such, it would be expected to strongly influence the properties of customary two-point correlation functions. We verify this by numerically studying two-point correlations. Further we find that this sort of pattern formation is not restricted only to the Sneppen model, but also occurs in other extremal models, such as the Zaitsev model for low-temperature creep [37] and the Bak-Sneppen model [38] of biological evolution, albeit in other quantities.

The plan of this paper is as follows. In Sec. II we introduce our model and discuss the connection with the problem of directed percolation, well established from earlier studies. In Sec. III, we discuss the correlations in the location of successive growth sites, a concept central to this paper because of its connection with pattern formation. In Secs. IV and V we define the pattern and present numerical results as well as an integral equation, which provides an understanding of this sort of pattern formation. We define a model for which the equation is exact and discuss how the approximation can be improved. In Sec. VI, we discuss the issue of temporal correlations with a view to seeing how they affect the pattern. In Sec. VII, we present our results for an ordinary two-point correlation function in our model and show that activity-centered pattern formation has to be taken into account in order to understand some features in it. Section

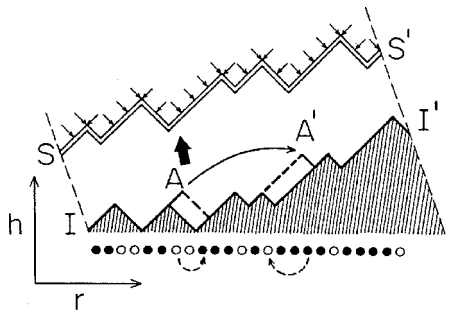

FIG. 3. The extremal bond model. The tilted interface II' advances along the extremal perimeter bond A and locally readjusts to align along the dashed line. At the next instant, the activity moves from A to A'. The corresponding configuration and local moves for the particle-hole model are also shown. SS' is a stopper, whose perimeter is fully occupied by diodes.

VIII deals with pattern formation in other extremal models and we conclude with a summary of our results in Sec. IX.

II. EXTREMAL MODEL OF INTERFACE DEPINNING

The extremal-model description of fluid-fluid interfaces in porous media is valid when the wetting is dominated by capillary forces, and thermal fluctuations are not important. In the extremal model, the interface advances along the weakest barrier just ahead of it. The appealing feature of the model is that it is self-organized critical; the dynamics, which involves searches for the global minimum at every step, automatically tunes the interface to a critical state at the depinning transition, without the necessity of fixing any external parameter. In the model proposed by Sneppen [24], the random medium is modeled by a square lattice in which the sites are assigned random numbers $f \in [0,1]$. The random numbers could signify, for instance, the pore sizes in a porous medium. The interface is a directed path on this lattice and grows only at that perimeter bond with the smallest value of the random number; after every such move, a local rearrangement process [39] ensures the absence of very large slopes.

Extremal dynamics has also been proposed to describe very different situations — for instance, the phenomenon of low-temperature dislocation creep [37,33], crack propagation [40], and biological evolution [38]. We will see in Sec. VIII that the sort of pattern formation we find in the interface model occurs in these models as well.

A. The extremal bond model

We study a modified version of the Sneppen model in this paper. In this version, hereafter referred to as the extremal bond model (EBM), the interface is taken to be a directed path on a square lattice (Fig. 3), with tilted cylindrical boundary conditions [41], which ensure that the mean slope is preserved. To every bond k on the lattice is preassigned a fixed random number f_k drawn from the interval [0,1]. The interface grows at that bond, in front of the interface, which carries the smallest random number. The local growth rules are the following: if the chosen minimal bond has a positive (negative) slope, the sequence of links with negative (positive) slope just below (on the left) also advances, as illustrated in Fig. 3. This preserves the length of the interface as would happen in situations with very high surface tension. The local dynamics of interface adjustment is similar to that for the low-noise Toom interface in [42]; the models are different in that the growth site is picked by the extremal rule in our case, while it is picked stochastically in the Toom interface model.

The EBM differs from the Sneppen model in that the length of the interface is a strict constant of the motion and the f_k's are associated with bonds rather than sites. While this modification does not change the values of any of the large-distance scaling properties of the Sneppen model, it has a few advantages. The interface aligns along directed spanning paths in a percolation problem, just as in the Sneppen model. In our case, the corresponding percolation problem is the diode-resistor percolation problem [43]. On the square lattice, it is dual to the directed bond percolation problem [44], which is relatively well studied. Another advantage is that the problem of interface growth in the EBM is conceptually simplified by the existence of a known one-to-one correspondence between the growing interface and a system of hard-core particles moving on a ring. The two-dimensional problem hence reduces to an effectively one-dimensional one. This also facilitates the numerics. The correspondence between the interface and the hard-core particles is detailed below.

Positive slope links of the interface are represented by particles ($n_j=1$) and negative-slope links by holes ($n_j=0$); see Fig. 3. The difference in height of the interface between sites j_1 and j_2 is given by $h_{j_2}-h_{j_1}=\Sigma_{j=j_1}^{j_2}(2n_j-1)$. In front of each link of the interface is a bond with a random number f assigned to it. Correspondingly, the site j with the particle (hole) representing this link carries a random number f_j. Just as for the interface, at each time step, activity is initiated at the site with the minimum f_j. The update rules for the interface translate to the following dynamics for particles and holes. If the site with minimum f_j contains a particle (hole), it exchanges with the first hole (particle) to the left (right). All sites hopped over, including the two which exchange the particle and hole, are refreshed by assigning a new set of f_j's. This corresponds to the fact that the updated portion of the interface moves ahead and meets a fresh set of f's on the square lattice. Because the number of positive slope links (and hence also the number of negative slope links) is conserved for the interface, in the particle-hole terminology, this implies that the number of particles is conserved. Hence we can define a density ρ for particles on the one-dimensional lattice. This density determines the mean slope $m=2\rho-1$ of the interface. An untilted interface corresponds to half filling. The reference direction for determining tilt is the easy direction of directed bond percolation on the square lattice, which is along the 45° line. Tilt refers to any density away from 0.5, which implies a slope different from 45°. The interface advances in a direction perpendicular to the direction of tilt and this translates to a nonzero current of particles on the ring.

B. Connection to diode-resistor percolation and directed percolation

Extremal models of interface depinning make use of a correspondence to the diode resistor percolation (DRP) and

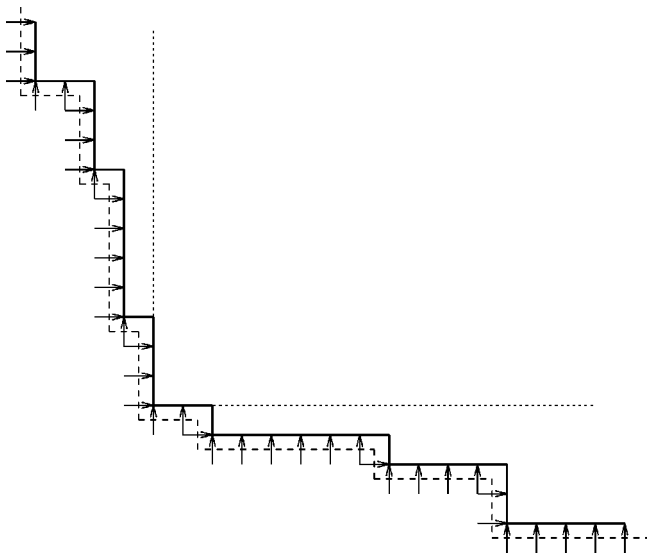

FIG. 4. The boundary of the region reachable from the origin in diode-resistor percolation. For a nonzero fraction of resistors, the opening angle of the region is larger than 90° as shown. The dashed line is an infinite path in the corresponding directed percolation problem on the dual lattice.

directed percolation (DP) problems to predict various properties of the interface. In view of this, it is useful to recall some facts about the DP and DRP processes.

In the directed percolation problem, bonds on a lattice are occupied with probability p. At some critical value p_c an infinite directed path of occupied bonds (in which every step is taken rightward or upward) first forms along a definite direction; on a two-dimensional (2D) square lattice, this is along the 45° direction. For $p>p_c$, The network of these infinite paths forms an infinite connected cluster. For directed bond percolation on a square lattice the value of p_c is known to be $\simeq 0.6446$ [44]. There are two distinct correlation lengths, $\xi_\parallel$ along the easy direction and $\xi_\perp$ transverse to it, both of which diverge as $p\to p_c$: $\xi_\parallel \sim (p-p_c)^{-\nu_\parallel}, \xi_\perp \sim (p-p_c)^{-\nu_\perp}$, respectively. The values of these exponents are known to be $\nu_\parallel \simeq 1.733$ and $\nu_\perp \simeq 1.097$ [44].

Suppose we have a single source point, and we ask which portion of the plane can be reached from it via occupied directed bonds. For $p>p_c$ this region is contained within a cone with opening angle $2\phi = \arctan(m)$ where m is the slope of the edge of the cone with respect to the 45° direction; the opening angle depends on p. This relation can be inverted to find the critical probability $p_c(m)$ viz., the probability at which a connection first appears along the direction with slope $m \neq 0$. Correlation lengths along and perpendicular to this direction have exponents $\nu_\parallel = 1$ and $\nu_\perp = 0.5$ [44]. We refer to the direction along 45° as untilted ($m=0$); any other slope is referred to as tilted.

In the diode-resistor percolation problem, every bond is occupied by a ''diode'' (a one-way connection) with a probability p or a ''resistor'' (a two-way connection) with a probability $1-p$. On a square lattice, the diodes all point up or right. Let us ask which regions of the plane are connected to a given source point. If $p=0$, a source point can reach the entire quadrant of which it is the left corner. As p decreases from 1 to p_c, the opening angle ϕ' of the connected region

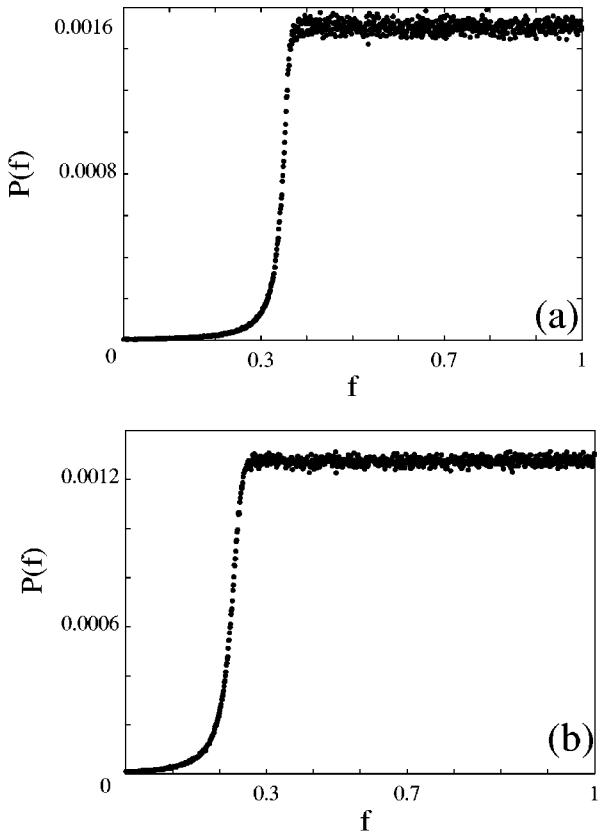

FIG. 5. The steady state probability $P(f)$ of having a bond with the value of the random number equal to f, in front of the (a) untilted and (b) tilted interface with $\rho = 0.75$, in the extremal bond model. There is a tilt dependent threshold below which the probabilty of finding a bond with that value is very low. A system of size 1000 was averaged over 10^7 configurations.

increases from $\pi/2$ to π; beyond this, the entire plane can be reached from the source point. The edge of the connected region is bordered by diodes pointing rightward and upward, which prevent it from spreading leftward and downward (Fig. 4).

On the 2D square lattice, DP and DRP are dual to each other [43]. The dual to a DRP configuration is constructed using the following rules. A diode in the DRP lattice is crossed by a diode in the dual lattice, whereas a resistor is crossed by an insulator (no connection) in the dual lattice. Thus we recover the directed percolation problem on the dual lattice. The opening angles of the cones in the two problems are related by $\phi + \phi' = \pi$.

In the EBM, the random medium is modeled by considering a square lattice with every bond assigned a random number f_k drawn from the interval $[0,1]$. For a certain trial value f^*, imagine occupying all bonds with $f<f^*$ by resistors, and the rest with diodes. We thereby generate a DRP configuration with $p=1-f^*$. When f^* takes on the value $1-p_c$, an infinite connected path of diodes is formed. Such a path is called a ''stopper,'' and is significant for the dynamics of the EBM, as a moving interface with no overall tilt will align with such stoppers from time to time [25]. When the interface aligns along a stopper, all the bonds in front of it are larger than $f_c = 1-p_c$ [Fig. 5(a)]. Similarly a tilted interface with slope m aligns along the edge of the cone with

the same slope and all the bonds in front of it are expected to have a value larger than $f_c(m)=1-p_c(m)$. Since $p_c(m) > p_c(0)$ for $m \neq 0$, $f_c(m) < f_c(0)$ [Fig. 5(b)]. Even when the interface is evolving between two stoppers, only a small fraction of its overall length actually is in between; the rest is still aligned with a stopper. The nonaligned fraction is expected to vanish in the thermodynamic limit. These expectations are confirmed by numerical studies of the EBM. As can be seen from the figures, the bonds in front of the interface are all mostly larger than a threshold value.

Consider an interface of slope m aligned along a critical DRP path of the same slope. It then moves forward by puncturing the path at the site with the least value of f, which for an infinite system is exactly $1-p_c(m)$. On piercing through, a portion of the interface grows and fills out a loop of the infinite cluster while the rest of it remains pinned. However, the interface motion within the loop is far from uniform. Just as the critical cluster at $p_c(m)$ impedes the growth of the interface on length scales of the order of the size of the system, near-critical clusters impede its motion at length scales of the order of but smaller than the loop size. One can think of these clusters as forming a finer network of connections within the network formed by the critical cluster at $p_c(m)$. While the interface is filling out a loop of the critical cluster, it encounters this finer mesh and as a result its motion is impeded temporarily. In what follows, we refer to these near-critical connections as ''sub-stoppers.'' A substopper can be characterized by the lowest value of f_k on it, say f^{ss}, and also by the typical length scale l over which it provides for effective pinning of the interface. These are related through $|f^{ss}-f_c(m)|^{-\nu_\parallel} \sim l$.

III. CORRELATIONS IN THE ACTIVE-SITE MOTION

The above description of the evolution of the interface, contained as it is by networks of substoppers and stoppers, makes it clear that there are strong correlations between successive points of growth or forward motion. These correlations extend from small length scales up to scales of the order of the system size. Figure 6 shows the plot of the location of the active site for 10 000 time steps for both the tilted and untilted cases. It can be seen that there are jumps on all scales in the active site position. The figure corroborates the description of interface motion given above. Region (1) is a typical instance of the interface filling out a loop of size l. It shows that there are jumps of all sizes up to a length l, bearing out the substopper picture. Region (2) on the other hand marks an instance when the interface has aligned along a stopper $p_c(m)$ and hence there are jumps of all sizes up to the system size.

More quantitatively, a measure of this long-ranged motion of the active site is the probability distribution $p(l)$ that two consecutive locations of the active site are a distance l apart. Figure 7 shows $p(l)$ for both the tilted and the untilted interface. In both cases, $p(l)$ decays as a power for large l: $p(l) \sim |l|^{-\pi}$.

In the untilted ($\rho=1/2$) case, $p(l)$ is a purely symmetric function because of $r \rightarrow -r$ symmetry. We find $\pi = 2.25 \pm 0.05$, which compares well with earlier determined values of π for the Sneppen model [34–36].

In the tilted case ($\rho \neq 1/2$), $p(l)$ is not a symmetric function (Fig. 7). As can be seen from the figure, there is a larger number of small jumps to the right, but more jumps of large magnitude to the left. It is convenient to separately analyze the even and odd parts $p_\pm \equiv [p(l) \pm p(-l)]/2$ in order to find the exponents. We find that the even part, $p_+(l)$, decays asymptotically as $p_+(l) \sim |l|^{-\pi_+}$ with $\pi_+ = 2.00 \pm 0.02$. The odd part $p_-(l)$ changes sign (as implied by the crossing of the curves in Fig. 7) and asymptotically follows $p_-(l) \sim |l|^{-\pi_-}$ with $\pi_- = 2.49 \pm 0.06$. We verified that the values of π_+ and π_- are the same for various $\rho \neq 1/2$. An interesting aspect of the function $p(l)$ for the tilted interface is that $\int l p(l) dl$ vanishes in the thermodynamic limit. In terms of the active-site motion, this implies that though, for the tilted interface, the short-ranged jumps of the active site are mostly along the tilt, there are enough long-ranged jumps in the opposite direction to balance this. The cancellation gets better as the thermodynamic limit is approached. The tilt of the interface, therefore, does not induce a net drift in the active site motion.

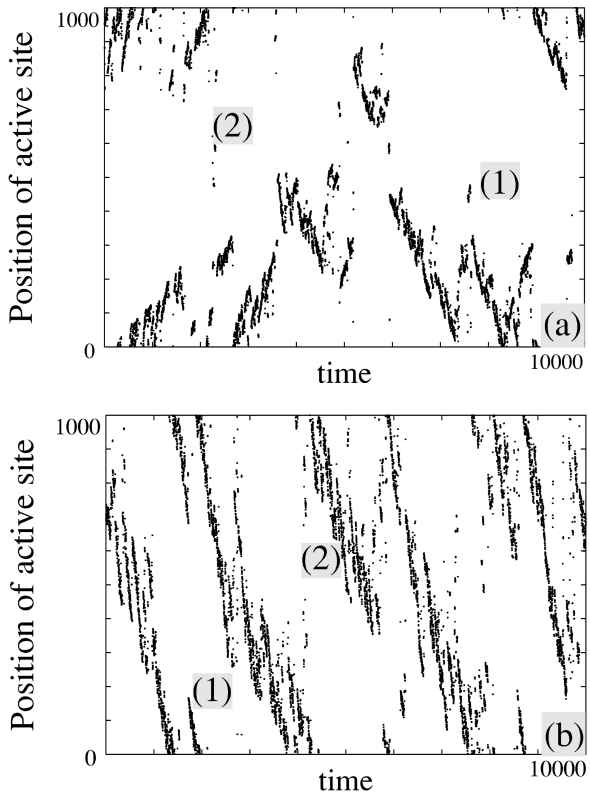

FIG. 6. The location of the active site on the lattice as a function of time (where time is incremented every time the active site is chosen for growth) for (a) the untilted and (b) the tilted interface. The region marked (1) is a typical example of a window in time in which the activity is localized in a region. In (2) the activity ranges through the whole system, corresponding to an instance when the interface has been pinned by a critical cluster at $p_c(m)$. Though the directionality of the active-site motion is evident in (b), this does not induce a net drift as mentioned in the text. The data displayed above are for $L=1000$.

Because of the close connection of the interface growth problem to DP, several exponents associated with the growth and structure of the interface are thought to be related to the DP exponents $\nu_\parallel$ and $\nu_\perp$ by scaling relations [45,35,36]. The exponent π in the untilted interface as well as the exponent

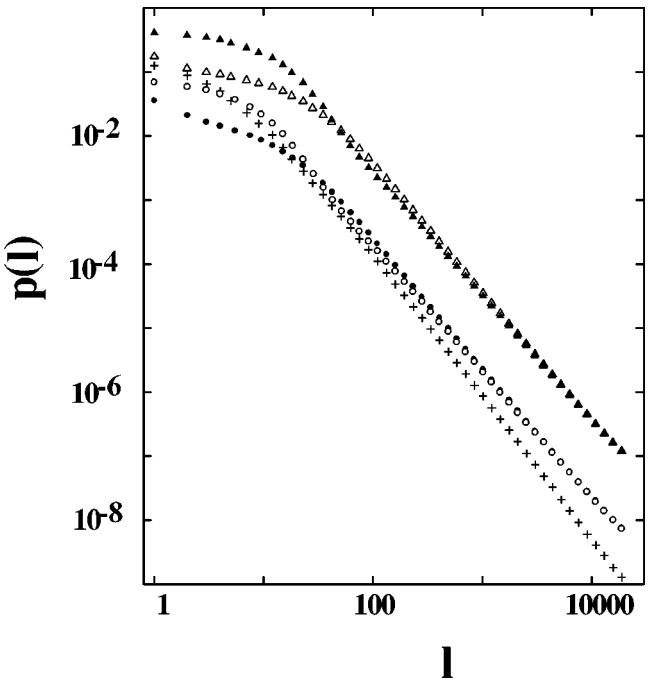

FIG. 7. Monte Carlo results for the probability distribution of the jump of the active site for three different densities, $\rho=0.5$ (plus sign), $\rho=0.75$ (circles), and $\rho=0.843\,75$ (triangles). If $\rho\neq0.5$, $p(l)$ is not a symmetric function and $p(l)$ and $p(-l)$ (both of which are shown in the figure in the two $\rho\neq0.5$ cases) do not coincide as they do for the symmetric case. While $p(l)>p(-l)$ for small l, the curves cross so that the situation is reversed for large jumps. The two curves asymptotically coincide with an asymptotic slope that differs from that for $\rho=0.5$. We used $L=65\,536$ and averaged over 3×10^9 configurations.

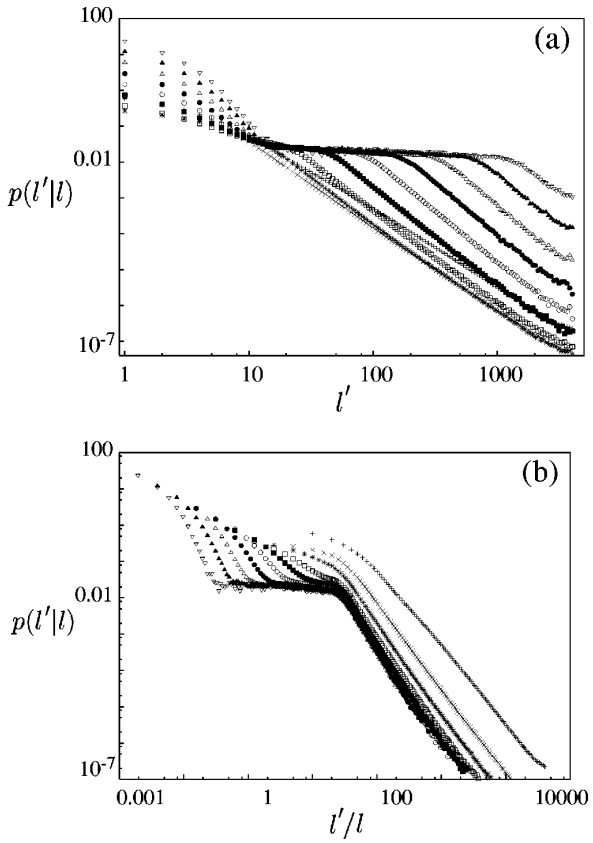

FIG. 8. (a) The function $p(l'|l)$ as a function of l'. l is logarithmically binned in powers of 2 and is maximum for the curve with the largest flat stretch. As can be seen in the figure, the flat stretches of the large-l curves coincide, peeling off at a value that is l dependent. (b) The function $p(l'|l)$ plotted as a function of l'/l. The curves coincide for large l indicating that the conditional probability is just a function of the ratio l'/l.

π_+ in the tilted case have been argued to be related to the DP exponents by the scaling relation $\pi=1+(1+\nu_\perp)/\nu_\parallel$ [36]. Besides this, for the tilted case, the exponents can also be obtained exactly [46,47].

As mentioned earlier, the function $p(l)$ does not contain all the information about the active-site motion. This is due to the presence of temporal correlations in the interface depinning model: the jump of the active site at the present instant is strongly correlated to the jumps before. As a result, what is needed is the full distribution function $p(l|l_{n-1}\cdots l_2|l_1)$, which is the conditional probability distribution that a jump of length l occurs at $t=n$ given that a jump of length l_1 occurred at $t=1$, a jump of length l_2 occurred at $t=2$ and so on. The probability distribution $p(l)$ is obtained by integrating out the other variables $l_1,l_2,\ldots,l_{n-1}$. In order to assess the importance of these temporal correlations, we numerically determined the conditional jump probability distribution $p(l'|l)$, the conditional probability that a jump of length l' occurs given that at the previous instant, the active-spot jumped a distance l. Figure 8(a) presents our numerical measurement of this function for the EBM. After the initial short-ranged decay, which is a result of the local backwetting move of the dynamics, the function is flat over a considerable range, and then decays as a power law. As evident in the figure, the range of the flat region depends on l but the value of the probability in the flat region becomes independent of l for large l. In Fig. 8(b) we show the scaling plot of $p(l'|l)$ obtained by plotting the curves as a function of l'/l. The function evidently approaches a scaling form for large l and l'. The scaling function is flat over a region and decays beyond as a power $\sim(l'/l)^{-\pi'}$. We expect $\pi'=\pi(\simeq2.25)$ to hold as $l'/l\to\infty$. Although the measured value of π' in the range shown is larger ($\simeq2.9$), the bending apparent in the lower right portion of the curve is consistent with an approach to the value π.

Qualitatively, the behavior of this function may be understood thus. If the active site jumps a distance l at the previous instant, one can think of the interface as pinned by a DP cluster with loops of average linear dimension $\sim l$. Most of the interface would then be pinned while a portion of it fills out a loop of linear dimension $\sim l$. This would imply that on average, any jump smaller than l is equally likely. On length scales larger than l the motion is like the original problem and hence the jump probability decays as a power law. This line of argument would imply that $p(l'|l)$ should be a scaling function of l'/l. Figure 8(b) bears out this expectation.

Another equivalent way of understanding the function $p(l'|l)$ is using the ''backward-avalanche'' technique introduced in [48]. A backward avalanche is defined as follows. If at time $s+S$ a random number f_k is picked as the minimum, the magnitude of the backward avalanche is S if at time s the random number picked was larger than f_k but for time s

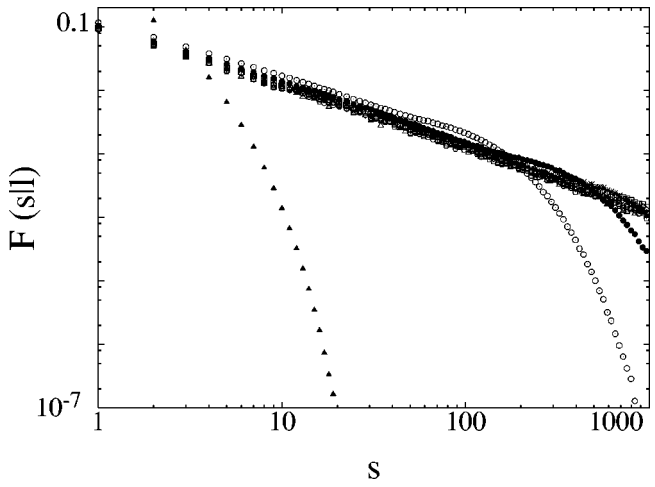

FIG. 9. The distribution $F(s|l)$ of durations of avalanches for jumps as defined in the text. For small l, $F(s|l)$ decays exponentially (filled triangles) as expected, since it is very unlikely that a larger jump does not immediately occur. As l increases, the cutoff for the decay increases (empty and filled circles) until for large enough l, the curves coincide, decaying as a power $\simeq s^{-1}$.

$+r$ for $r<S$ the value of the random number picked was smaller. That is, one goes back in time to the first instant when the random number picked is larger than the present one and this interval of time is the magnitude of the backward-avalanche initiated at the present instant. If the active site hopped a distance l in the previous instant, this would imply that the size of the spatial region affected by the backward avalanche initiated at the previous instant is $\sim l$. At the next time step any of three possibilities can occur. If the random number picked is *smaller* than the previous one, then the active site necessarily lies in the local region, which has just been affected by the move. If the random number picked is larger, then either the random number picked belongs to the same backward avalanche as the previous one, or it belongs to a bigger one (which therefore encompasses the previous one). In the former case, the active site is equally likely to hop anywhere in the region affected by the present backward avalanche [36,48] and hence the function is flat up to a length $\sim l$. In the latter case, active-site hops are in general larger, since the encompassing backward avalanche is larger. The probability of having the active site hop a distance $l_1>l$ is then related to the probability of finding a backward avalanche of this spatial extent, and hence decays as a power law.

Another indication of the correlation in the jumps of the active site is the following quantity, which is the analog of an avalanche, for jumps (Fig. 9). Let the avalanche be initiated at an instant s by a jump of magnitude l of the active spot. The ''jump avalanche'' lasts as long as consecutive jumps in the active site are less than l. That is, the avalanche is of duration S if at time s the active site hopped a length l, and for S consecutive instants after that, the hops in the active site are smaller than l until at the $(S+1)$th instant, it hopped a distance greater than l. The analog of this quantity for random numbers was first defined for models in the nonwetting invasion percolation regime [31,32] and later also measured for the Sneppen model [45,35,36]. The jump avalanche is a strong indication of the correlation in successive jumps of the active site. As Fig. 9 indicates, the function falls off as a slow power law. This is an indication of the long-term memory in the system, as the function would decay exponentially if successive jumps had not been correlated.

IV. PATTERN FORMATION IN THE INTERFACE DEPINNING MODEL

A. Definition

As discussed in the previous section, the motion of the active spot in this model is very correlated. One can then ask whether this motion reorganizes the shape of the interface (or equivalently the arrangements of particles and holes in the particle model corresponding to the EBM) in any specific way. Below we will show that the correlated motion of the growth spot in this model leads to the formation of a pattern in height gradients (or equivalently the density of particles) of the interface.

The defining Eq. (1) for height gradients can be written in terms of densities as

$$\Psi(r)=\langle n(r+R(t))\rangle-\rho. \tag{2}$$

Here $n(r)$ is the density at site r and the angular brackets denote a time average in the steady state.

This pattern is linked to the formation of a structure that is very different from normal space-fixed patterns because it refers to an origin $R(t)$, which is moving around. In fact it can be discerned *only* when the origin moves. An ordinary space fixed average is translationally invariant and satisfies $\langle n(r)\rangle=\rho$ for any site r. Since the pattern is centered around the site of activity, we will refer to it as the ''activity-centered pattern'' (ACP).

B. Numerical results

We studied $\Psi(r)$ by Monte Carlo simulation in the particle-hole representation. We studied systems of size L ranging from 2^{10} to 2^{16}. The system was allowed to evolve through 10^6-10^7 configurations before measurements were made. In order to speed up the algorithm to locate the site with the minimum f, we used a logarithmic-bin search procedure. Steady state averages were computed using $\sim 10^8$ configurations. While this number of configurations was averaged over to get an accurate estimate of the decay exponent, even an average over about 100 configurations indicates the presence of a strong density inhomogeneity clearly.

In the untilted case, the height profile is an even function [Fig. 1(a)] and $\Psi(r)$ is an odd function [Fig. 10(a)] decaying asymptotically as a power law $|r|^{-\theta}$ with $\theta=0.90\pm0.03$ (Fig. 10, inset). In the tilted case as there is no $r\rightarrow -r$ symmetry, $\Psi(r)$ does not have a definite parity [Fig. 10(b)]. It is useful to separately analyze the even and odd functions $\Psi_{\pm}(r)\equiv[\Psi(r)\pm\Psi(-r)]/2$. The odd part decays as $\Psi_{-}(r)\sim|r|^{-\theta_{-}}$ with $\theta_{-}=1.04\pm0.05$ (Fig. 10, inset). The even part $\Psi_{+}(r)\approx -b(L)+a|r|^{-\theta_{+}}$ where $\theta_{+}=0.46\pm0.05$ and $b(L)\rightarrow 0$ as the lattice size $L\rightarrow\infty$ (Fig. 11).

The density profiles of Fig. 10 correspond to the height patterns shown in Figs. 1 and 2. Qualitatively, the reason for this time-averaged structure of the height profile can be seen as follows. In the untilted case, on average, the active site is

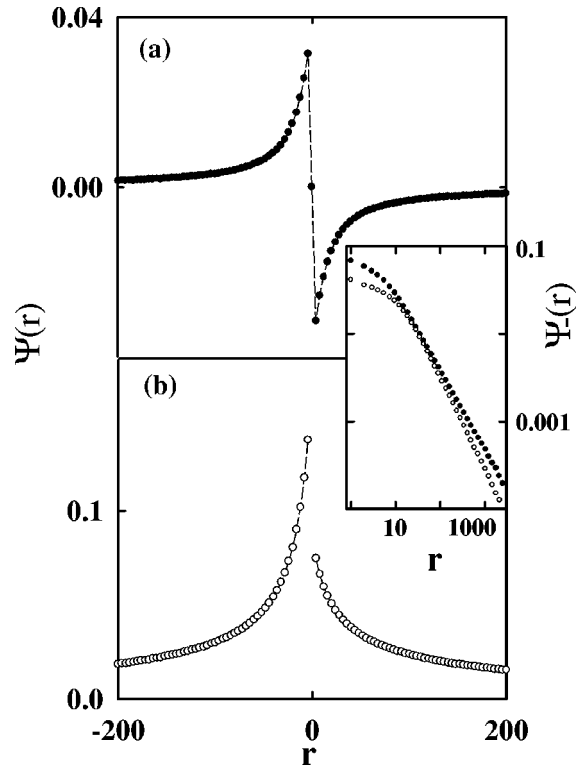

FIG. 10. Density profiles in the (a) untilted ($\rho=0.5$) and (b) tilted ($\rho=0.75$) cases. Note that in (b), the value at the origin is larger than 0.75, indicating that the active site is more than nominally likely to have a particle, because of the bootstrap effect discussed in the text. While (a) is an odd function of r, (b) has no parity and the even and odd parts can be studied separately. The inset shows the odd part of the profile in the untilted (filled circles) and tilted (open circles) cases. Both decay as power laws though with differing exponents. We used $L=16\,384$ and averaged over 10^8 configurations.

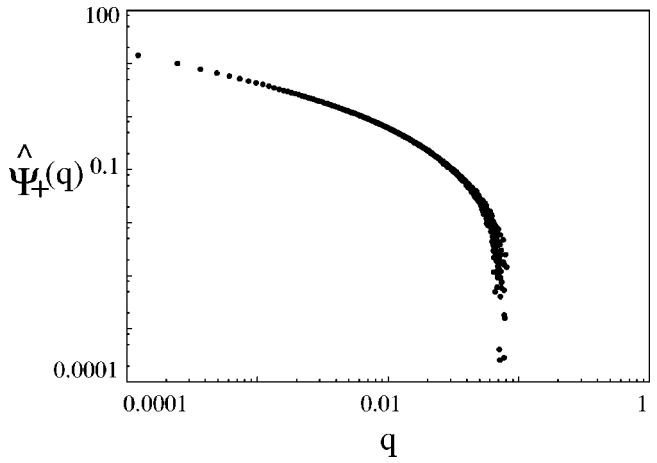

FIG. 11. A log-log plot of the Fourier transform of the even part of the density profile in the tilted ($\rho=0.75$) case, for the data appearing in Fig. 10. At low q the function decays as a power $\simeq q^{-\phi}$ with $\phi\simeq 0.54$ implying that at large r, the behavior is a power law with decay $r^{-(1-\phi)}$.

located at the peak [Fig. 1(a)] where f_k's that have not been sampled earlier are most likely to occur; such a region is thus more likely to contain small values of f. In the tilted case there is, in addition, a bootstrap effect at work. If $\rho\geqslant 0.5$, the active site is more likely to contain a particle. Given the dynamics, regions to the left are more often refreshed, making the active site likely to move in this direction and find itself amidst a particle cluster. The directionality of the active site motion is evident in Fig. 6. This leads to densities higher than ρ on both sides of the active site [Fig. 10(b)] for ρ sufficiently different from 0.5. That particles are picked more often than would be expected on the basis of the nominal density is evident from the fact that the value of the density at the active spot is larger than ρ. For the density pattern in Fig. 10(b), which corresponds to $\rho=0.75$, the value of the density at the origin is $\Psi(0)=0.84$.

In the next section we develop an approximate theoretical description for the exponents describing the decay of the pattern in terms of the exponent π, which describes the long-ranged hops of the active site.

V. THE INTEGRAL EQUATION FOR PATTERN FORMATION

As discussed in the previous section, a pattern in height gradients or densities is formed in the interface depinning model. It is related to the motion of the active site, which rearranges the particles and holes in its wake. For example, if the active site were to remain stationary at a given site for a certain length of time, the dynamics is such that it would build up a pileup of particles to the left of the site and a pileup of holes to the right, i.e., it would create a density shock around itself. In this section, we write down an integral equation that provides a description of the pattern in terms of $p(l)$, the probability that the active site hops a length l in consecutive instants, as well as the local dynamics of interface readjustment.

If the pattern is centered at $R(t)$ at time t, the dynamics causes two changes at the next instant: (i) A short-ranged readjustment of the interface changes the profile near $R(t)$. The average density change at site $R(t)+r$ is modeled through a density-increment function $\Phi(r)$, which is short ranged. (ii) The active site jumps a distance $l\equiv R(t+1)-R(t)$. Since the pattern is centered at the active site, the result of (i) followed by (ii) is that the average profile reproduces itself, except that it is centered at the shifted site $R(t)+l$. Both effects are incorporated into the integral equation

$$\Psi(r)=\int_{-\infty}^{+\infty}[\Psi(r-l)+\Phi(r-l)]p(l)dl. \qquad (3)$$

This equation can be solved using Fourier transforms. In particular, the long-distance behavior of the pattern $\Psi(r)$ is related to the decay of $p(l)$ for large l, resulting in a scaling relation for the exponent θ in terms of the exponent π. The details of the analysis are given in Sec. V B below.

However, this equation provides only an approximate description. To understand the nature of the approximation made, we define a ''Lévy-flight model,'' which is similar in spirit to the models of [20,34]. As in these models, there is no explicit quenched disorder, but the effect of disorder is modeled by a long-ranged jump probability distribution. For this model, we show that the integral equation (3) holds exactly. Further, we can gain considerable insight into the

mechanism of activity-centered pattern formation by studying the effect of different decays of the jump function $p(l)$ within the Lévy-flight model.

A. Derivation of the integral equation for the Lévy-flight model

The Lévy-flight model is defined as follows. Consider a one-dimensional lattice with particles and holes. We assume that a jump probability distribution $p(l)$ is specified *a priori*: if at $t=0$ the active site is located at a site r, at the next instant, it can lie a distance l away (i.e., at $l+r$) with a probability $p(l)$. Evidently there are no temporal correlations in this model, since at every instant, the jump length is chosen afresh from the distribution $p(l)$. Spatial correlations in the active-site motion are, however, built in by hand since $p(l)$ is given. Once a particle or hole is picked for update, the local rules are assumed to be the same as in the extremal bond model, i.e., the particle (or hole) exchanges position with the nearest hole (or particle) to the left (or right).

We now derive an integral equation starting from the master equation for the Lévy-flight model. We first define a configuration i to be a set of integers $(\{n_i(r)\},R_i)$ $r=1,\ldots,N$ where N is the size of the lattice and R is the current position of the active site. The variables $n(r)$ can take the values 0 or 1 depending on whether the site r is occupied by a particle or is empty and R can take any value between 1 and N. The total number of states is, therefore, $N_T=N\times {}^{N}C_{N_p}$ where N_p is the number of particles. In the usual manner, we characterize the steady state by a column vector $|P\rangle$. The entries of this column vector are the probabilities P_i for the configuration i where $i=1,\ldots,N_T$. To obtain the steady state, we need to solve the master equation $d|P\rangle/dt=W|P\rangle$ where W is an $N_T\times N_T$ matrix connecting the different states. The dynamics that connects different states is the following: The particle (hole) at R is exchanged with the nearest hole (particle) to the left (right) as specified earlier. Subsequently the active site now hops from R to $R+l$ with a probability $p(l)$. The diagonal elements of the matrix are $W_{ii}=-1$. The off-diagonal elements are given by $W_{ij}=p(l)$ if configuration i is connected to configuration j by an elementary update and a jump of the active site of length l and by $W_{ij}=0$ otherwise. Since the probability $p(l)$ is normalized $[\Sigma p(l)=1]$ the sum $\Sigma_i W_{ij}$ for each column of the matrix adds up to 0. This is a requirement for any stochastic matrix.

Every configuration i can go to N other configurations. Each of these differ from i in the positions of the particle and hole exchanged in the elementary update move, and also in the position of the active site. Similarly there are N configurations that feed into any configuration i. The construction of these configurations is very similar to that carried out in the case of the low-noise Toom interface and related models [49]. However, unlike in that case, here the transition probabilities are not all the same. As a result the steady state here is very different from the product-measure steady state found in [49] and is difficult to characterize for general $p(l)$.

However, we are able to characterize one aspect of the steady state by defining a quantity Ψ in the following manner:

$$\Psi(r)=\sum_{i=1}^{N_T} P_i n_i(r+R_i)-\rho. \tag{4}$$

That is, we add up the densities at a site r for each configuration that occurs in the steady state, having first shifted the origin separately in each configuration so that the site r for every state is one that lies r away from the active site. From this is subtracted the average density ρ. The above equation is equivalent to Eq. (2), with the time average in the latter being replaced by a weighted sum over configurations here.

From examination of the W matrix, it is clear that in the case that $p(l)$ is a constant independent of l (as in ordinary stochastic processes), all the P_i's are equal. As a result, from the definition, the ACP vanishes. However, while this is a sufficient condition it is not necessary. There are instances (see Sec. VIII) when special symmetry considerations rule out any pattern formation. However, the presence of an ACP definitely implies the presence of a nontrivial $p(l)$; a pattern indicates correlations in the active-site motion.

We will now derive Eq. (3) for the Lévy-flight model. Note that the probability $P_i=\Sigma_l p(l)\Sigma'_{j\to i}P_j$ where the prime on the summation implies that only those configurations j are considered in which the active site is l sites away from its position in i. Further j should transform to i when the active site is updated. This equation follows from the master equation. The sum is over all l's.

We can now substitute this in the right-hand side of Eq. (4):

$$\Psi(r)=\sum_l p_l \sum_i n_i(r+R_i)\sum_{j\to i}{}' P_j-\rho. \tag{5}$$

The density at site r in the configuration i is multiplied by the sum of the probabilities of those configurations that lead to it after a local update: a local exchange of a particle and hole, and a subsequent jump of the active site of length l. Hence we can write

$$n_i(r+R_i)=n_j(r+R_i-l)+\phi_j(r+R_i-l). \tag{6}$$

Here $\phi(r)$ is a short-ranged function [this is related to the ''density-increment'' function appearing in Eq. (3)], which depends on the local update rules. It is defined by Eq. (6) and is the difference between the two configurations i and j, which are related by an update. This function is the same for this model as for the bond model (Fig. 12) since it depends only on the local update rules. In the EBM, it is a short-ranged function whose range is determined by the average length of particle and hole hops. Later in this section we will comment on circumstances in which this function can become long ranged.

Substituting Eq. (6) in Eq. (5), we find that the right hand side can be rewritten as

$$\Psi(r)=\sum_l p(l)\sum_i [n_i(r-l)+\phi_i(r-l)-\rho]P_i. \tag{7}$$

Using the definition of $\Psi(r)$ again, we finally obtain the integral equation (3) for $\Psi(r)$ in terms of $p(l)$,

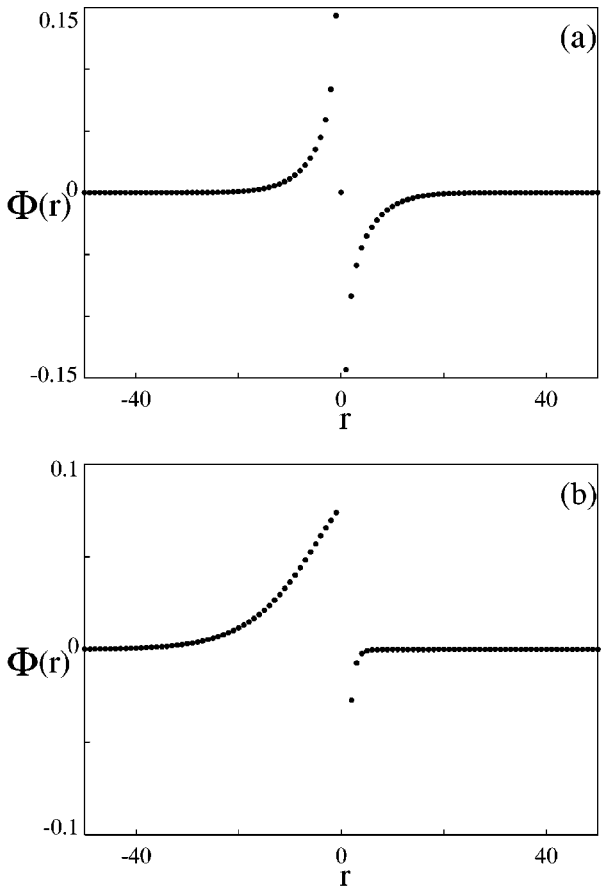

FIG. 12. The density-increment function $\Phi(r)$ in the EBM for (a) untilted and (b) tilted cases. Due to particle-hole symmetry, the function is a short-ranged purely odd function in (a) while it has no specific parity in (b). In both cases, however, $\int \Phi(r)dr=0$ from particle-hole conservation. We used $L=16\,384$ and averaged over 16×10^8 configurations.

$$\Psi(r)=\sum_l p(l)[\Psi(r-l)+\Phi(r-l)]. \tag{8}$$

Here we have defined an averaged function $\Phi(r)=\Sigma_i P_i \phi_i(r)$. From particle conservation, it follows that $\int \Phi(r)dr=0$. For the symmetric case of half filling, $N/2$ particles and $N/2$ holes, the function Φ is strictly an odd function. However, this does not hold when the number of particles is not equal to the number of holes [Fig. 12(b)].

Thus we have been able to show that the integral equation (2) is valid for the Lévy-flight model. From the nature of the model, it is clear that while spatial correlations in the active site motion are built in by hand, there are no temporal correlations in the length of subsequent hops of the active site. Therefore the integral equation is exact only in such a case. In the next section, however, we carry over some of the predictions of the integral equation to the EBM and find that in some cases, it tallies quite well with numerical results. In Sec. VI, we discuss briefly how to generalize Eq. (8) to include temporal correlations such as are present in the EBM.

B. Analysis of the integral equation

We now investigate the predictions of Eq. (3) for $\Psi(r)$ in terms of a given active site hopping probability $p(l)$ and the short-ranged readjustment function $\phi(r)$. We solve the equation using Fourier transforms. Defining $\hat{\Psi}(q) \equiv \int_{-\infty}^{+\infty} e^{2\pi i q r}\Psi(r)dr$, etc. we find

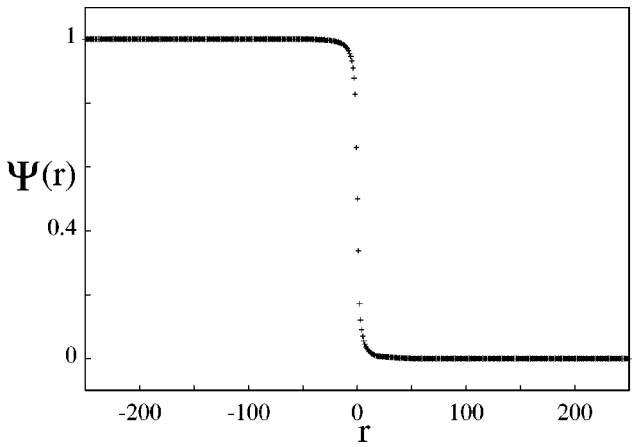

FIG. 13. The activity-centered pattern $\Psi(r)$ in the Lévy flight model for which $p(l)$ decays rapidly as $l^{-6.0}$. As evident in the figure, there is a near complete segregation of particles and holes about the active site. A system of size 1024 was considered and $\sim 10^5$ configurations were averaged over.

$$\hat{\Psi}(q)=\frac{\hat{\Phi}(q)\hat{p}(q)}{1-\hat{p}(q)}. \tag{9}$$

Since we are mainly interested in the $q\to 0$ behavior of Eq. (9), we do not need the full functional form of $\hat{\Phi}(q)$ but only the leading order behavior.

Given a function $p(l)$ the integral equation predicts a corresponding $\Psi(r)$. The large-distance behavior of the ACP thus depends on whether $p(l)$ is short or long ranged. We consider now three different cases for the function $p(l)$ and solve for $\hat{\Psi}(q)$ using Eq. (9). We substantiate the predictions of the equation by numerically simulating the Lévy-flight model.

Case 1: Consider first the case of an infinite-ranged $p(l)$. The simplest case is when $p(l)=1/N$, where N is the number of sites in the lattice. This case corresponds to usual stochastic processes. In this case $\hat{p}(q=0)=1$ and $\hat{p}(q\neq 0)=0$. This implies that $\hat{\Psi}(q)=0$ for $q\neq 0$ and is therefore a very short-ranged function in space.

Case 2: Consider now the case when $p(l)$ is a short-ranged function. We will consider the case when it is symmetric and hence for low $q\hat{p}(q)\sim q^2$. Substituting this in Eq. (9) we find that $\hat{\Psi}(q)\sim \mathrm{sgn}(q)/|q|$. This implies that $\Psi(r)\sim \mathrm{sgn}(r)$. The particles and holes separate out completely and the active site is located at the boundary between the two. This is easy to understand if we consider the limiting case when the active site is totally stationary. In this case, the action of the dynamics is to move all the particles from the right of the active site to its left. Eventually, this leads to a total separation of particles and holes. This picture is modified only slightly when the active site executes a localized motion about any lattice site, and hence for a short-ranged $p(l)$ (Fig. 13).

Case 3: We now come to the case of interest for the interface depinning model, i.e., when $p(l)$ decays as a slow power law. If $p_+(l)=1/|l|^{\pi_+}$, Eq. (9) predicts that $\Psi(r) \sim \mathrm{sgn}(r)|r|^{\theta_-}$. The exponents π and θ_- are related by the scaling relation $\theta_- + \pi_+ = 3$. This is to be compared with the numerical estimate $\theta_- + \pi_+ = 3.15$ for the extremal bond model in the untilted case. Consider now the case when none of the functions $p(l), \Psi(r)$, and $\Phi(r)$ has a definite parity. This is relevant for the tilted interface in the Sneppen model. Since $\Phi(r)$ is short ranged, $\hat{\Phi}(q) \approx i\phi_1 q + \phi_2 q^2$ as $q \to 0$. There is no ϕ_0 term, as the elementary step of hopping a particle or hole conserves particle number, implying $\int \Phi(r) dr = 0$. The $q \to 0$ behavior of $\hat{p}(q)$ is determined by the asymptotic power-law decays of the even and odd parts $p_\pm(l)$ as $|l| \to \infty$. Thus we have $\hat{p}_+(q) \approx 1 - A|q|^{\pi_+ - 1}$. We might have expected $\hat{p}_-(q) \approx Bq + C\,\mathrm{sgn}(q)|q|^{\pi_- - 1}$, but in fact the mean velocity $\int lP(l)dl$ of the active site vanishes (as mentioned in Sec. III) implying $B=0$. Thus the integral equation predicts that to leading order both $\Psi_+(r)$ and $\Psi_-(r)$ decay as powers $\sim |r|^{-\theta_\pm}$, with

$$\theta_+ + 2\pi_+ - \pi_- = 3$$

and

$$\theta_- + \pi_+ = 3.$$

The prediction $\pi_+ + \theta_- = 3$ compares quite well with the numerically determined values 3.04 for $\Psi_-(r)$ in the tilted case. For $\Psi_+(r)$, however, the numerically determined value of $\theta_+ + 2\pi_+ - \pi_- (\simeq 1.97)$ deviates substantially from the predicted value 3. The likely reason behind the discrepancy is explained in the next section.

C. Drawbacks of the approximation

The integral equation (2) is exact for the Lévy-flight model, but only approximate for the EBM of interface depinning. Here we briefly run over the nature of the approximations made, and possible directions for improvement.

One sort of approximation is the neglect of correlations between lengths of successive jumps; as we saw in Sec. III, these correlations are very marked. The extension of the integral equation to include such correlations is discussed in Sec. VI B.

As noted in Case 3 of Sec. V B for tilted interfaces ($\rho \neq 0.5$), the pattern is not well represented by Eq. (2) even qualitatively. The reason for this is that the $\rho \neq 0.5$ pattern in the EBM is formed due to a feedback effect, which is missing in the Lévy-flight model. If $\rho > 0.5$, then within EBM dynamics, particles (or holes if $\rho < 0.5$) are picked more often than just ρN_{try} times in N_{try} tries. This condition is not incorporated in Eq. (3) at all. To test how important this effect is, we simulated the Lévy-flight model with the further constraint that if a site chosen for growth does not contain a particle, it is discarded and the search is continued until a site containing a particle is found. This leads to a pattern that more closely resembles that in the $\rho \neq 0.5$ EBM, in that the even part of the pattern is much more prominent than the odd part (see Fig. 14).

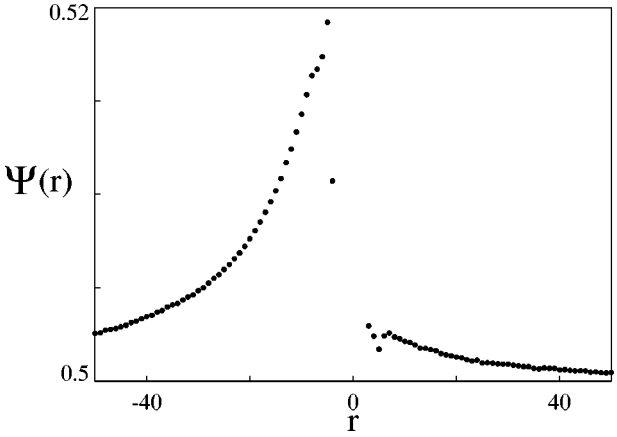

FIG. 14. The activity-centered pattern $\Psi(r)$ for a Lévy flight model with the further constraint that only sites containing particles are chosen. The pattern generated with these rules resembles $\Psi_+(r)$ in the EBM more closely than if the rules were implemented without the constraint. This fits in with our conjecture as to why the integral equation does not describe the even part of the pattern.

Another point to note is that we have always taken the density-increment function Φ to be short ranged. Insofar as we are interested in the EBM, this is certainly so. However, in the Lévy-flight model, any power larger than 3 results in a pattern like the one shown in Fig. 13, with a segregation of particles and holes and not one decaying as a power as predicted by the integral equation. The reason for this is that in this case, the mean squared distance $\langle R^2(t) \rangle$ covered by the active site in time t is finite. Hence for a large system, this is like a short-ranged motion and leads to particle hole segregation. In the process, as particle clusters build up, the density-increment function is no longer short ranged.

Lastly, while in the EBM, the probability distribution of jumps $p(l)$ arises naturally from the dynamics, in the Lévy-flight model we put in the spatial correlation in the active site motion by hand. In the following section, we try to remedy this point by modifying the integral equation by writing a set of coupled equations.

D. The coupled equations

A drawback of the Lévy-flight model is that the function $p(l)$ has to be supplied from the outside. We try to rectify this by writing a set of coupled equations that predict $\Psi(r)$ and $p(l)$ in terms of each other.

In order to do this, we need to understand the probability that a certain portion of the pattern is visited by the active site. In the EBM, the site visited last has the largest probability of being visited again since it is most likely to have the least random number. The more often a region is visited, the more the random numbers associated with sites in that region are refreshed and hence the more likely it is that the minimum random number lies in that region. Since the dynamics creates a particle excess on the left of the active site and a corresponding paucity on its right, a density shock is built up in that region. The extent of the shock is directly proportional to the length of time spent by the active spot in that region. The larger the shock, the larger the density difference, and hence the larger the derivative of Ψ. Hence the effect of a region being visited a large number of times is

precisely that $d\Psi/dr$ is large. But as explained above, the larger the number of times a site is visited, the larger is the probability of its being visited again. Thus we conjecture that the probability of visiting a region a distance l away from the active site is proportional to the magnitude of $d\Psi/dr$ in that region, and write the following equations:

$$\Psi(r)=\int dl p(l)[\Psi(r-l)+\Phi(r-l)] \tag{10}$$

and

$$p(l)=\mathcal{N}^{-1}\left|\frac{d\Psi}{dr}\right|_{r=l}, \tag{11}$$

where $\mathcal{N}=\int|d\Psi/dr|$ is the appropriate normalizing factor.

Equation (10) is the integral equation that we derived in the last section. Equation (11) now defines $p(l)$ in terms of the pattern Ψ. The details of the dynamics of particle-hole exchange in this model make this a reasonable premise as explained above.

Let us compare the results of the coupled equations with those for the untilted interface. If $\Psi(r)\sim|r|^{-\theta}$ and $p(l)\sim|l|^{-\pi}$, we saw in Sec. V B that Eq. (10) implies relation $\pi+\theta=3$. Further, Eq. (11) predicts the relation $\theta+1=\pi$. The solution is $\pi=2$ and $\theta=1$. This compares quite well with the value of the exponents $\pi=2.25\pm0.05$ and $\theta=0.9\pm0.03$ found numerically for the EBM.

VI. TEMPORAL CORRELATIONS IN THE INTERFACE DEPINNING MODEL

A. Time dependence of the pattern

The pattern, as defined earlier, is obtained by a straight time average over all configurations, taking care to shift the origin appropriately at every instant. It is interesting to ask how the pattern changes if we consider only those configurations that occur after very large jumps of the active site (or equivalently, only those configurations for which the minimum random number is very close to the largest possible). A strong dependence of the pattern on the configurations averaged over is evident in Fig. 15. The pattern gets more squashed as the jumps in the active site leading to the configuration get larger. This implies that the pattern ceases to exist at stoppers and builds up again as the interface pierces through. The actual dynamics of pattern collapse and buildup is an interesting subject for further study.

It should be recalled that long jumps occur much more infrequently than short jumps (Fig. 7); the probability of occurrence of a stopper is thus very low. The time average in the definition of the pattern [Eq. (1)] is dominated by configurations between stoppers (when the active site is moving within the loops of the directed percolation network), rather than those at stoppers (when the active site is on the backbone of the network).

B. A Hierarchy of integral equations

The integral equation (3) can be modified to include correlations in time. To do this, we enlarge the definition of a configuration i to include the active site at the previous instant as well. Now the off-diagonal elements of the transition matrix elements $W_{ij}=p(l'|l)$ if configuration j has resulted as a consequence of a jump of the active site of length l and is connected to configuration i by an elementary update and a jump of the active site of length l'. The function $p(l'|l)$ is just the conditional jump probability already introduced in Sec. III.

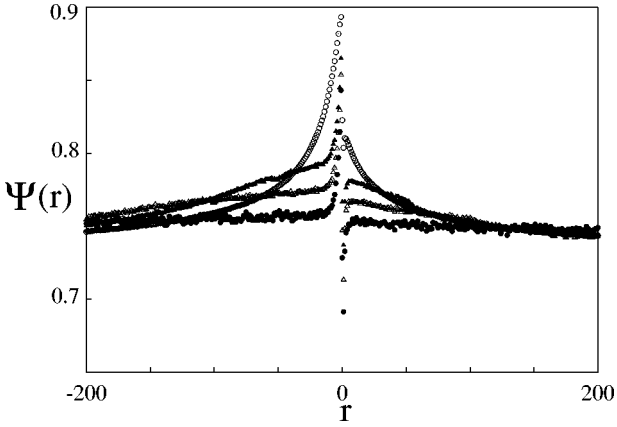

FIG. 15. Evidence for the dependence of the ACP on the length of the previous jump of the active site. $\Psi(r)$ is shown with time-averaging done over (1) all configurations (open circles), (2) only configurations resulting after a jump in the active site of magnitude 50 (filled triangles), (3) only configurations resulting after a jump of length 100 (open triangles) and (4) only configurations resulting after a jump of length 300 (filled circles). As is evident, the pattern gets more and more squashed until it barely exists in (4). A system of size 1024 was used and $\sim10^6$ configurations were averaged over.

Following the same procedure as before, we get an equation for $\Psi_{l'}(r)$, the pattern resulting from an active site hop of length l:

$$\Psi_{l'}(r)=\sum_{l} p(l'|l)[\Psi_l(r-l')+\Phi_l(r-l')]. \tag{12}$$

Keeping correlations up to one time step back gives the pattern a nontrivial dependence on the jump length l'. The integral equation (3) gives only a trivial dependence of $\Psi(r)$ on l'.

This procedure can be further generalized by going back one more step in time and keeping the location of the active site two instants back.

This leads to an equation of the following sort:

$$\Psi_{l,l_1}(r)=\sum_{l_2} p(l|l_1|l_2)[\Psi_{l_1,l_2}(r-l)+\Phi_{l_1,l_2}(r-l)],$$

where $p(l|l_1|l_2)$ is the conditional probability that the active site hops a length l given that at the previous instant it hopped a distance l_1 and in the instant before that, a length l_2. Similarly, $\Psi_{l_1,l_2}(r)$ is the pattern formed when averaged over configurations that result after two consecutive jumps of l_1 and l_2, respectively.

Here $\Sigma_{l_1}\Psi_{l,l_1}(r)=\Psi_l(r)$. Keeping the time sequence of jumps leads to an infinite hierarchy of equations:

$$\Psi(r)=\sum_{l}\sum_{l'} p(l'|l)[\Psi_l(r-l')+\Phi_l(r-l')], \tag{13}$$

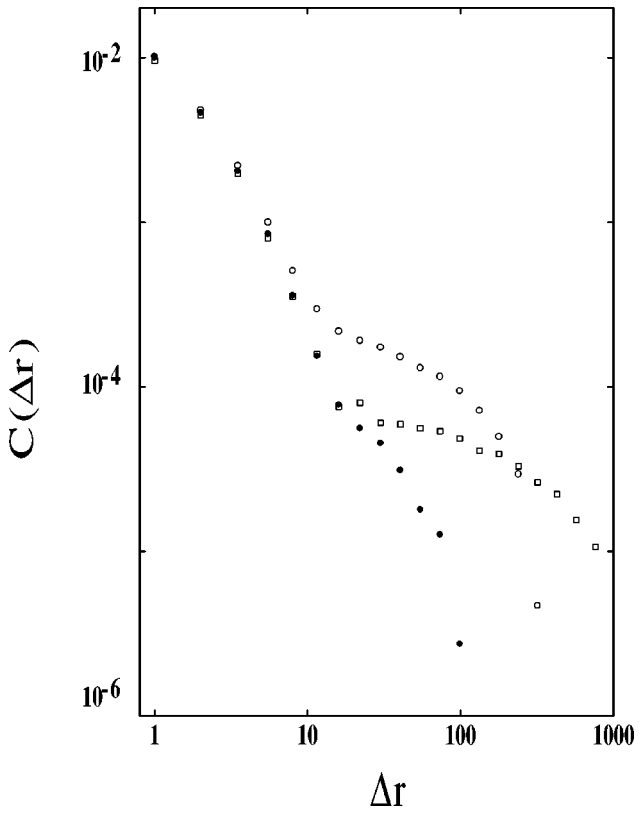

FIG. 16. Two-point density-density correlation function for $L=4096$ (open circles) and for $L=16\,384$ (squares). The saturation value is reduced strongly (filled circles) on subtracting the contribution of the ACP. This lends support to the idea that the one-point correlation function defined by the ACP enters the definition of the connected part of the two-point correlation function. The data were obtained by averaging over 10^6 configurations.

$$\Psi_l(r)=\sum_{l_1,l_2} p(l|l_1|l_2)[\Psi_{l_1,l_2}(r-l)+\Phi_{l_1,l_2}(r-l)], \tag{14}$$

$$\Psi_{l_1,l_2}=\cdots. \tag{15}$$

The integral equation (3) corresponds to curtailing this hierarchy at the first step by assuming that $\Psi_l(r-l')\sim\Psi(r-l')$ and $p(l'|l)=p(l')$.

VII. TWO-POINT CORRELATION FUNCTIONS IN THE INTERFACE DEPINNING MODEL

The activity-centered pattern $\Psi(r)$ defined in Eq. (1) is a one-point correlation function, defined with respect to an erratically moving origin. As a result, it has a strong effect on the customary, space-time averaged two-point correlation function

$$C(\Delta r)\equiv\{\langle n(r')n(r'+\Delta r)\rangle\}-\rho^2.$$

Here r' is a fixed site on the lattice, $\langle\cdots\rangle$ stands for a time average, and $\{\cdots\}$ stands for an average over all sites r'.

Numerical results for $C(\Delta r)$ for a tilted interface show that it saturates at a value $C^{\rm sat}$, which decreases with increasing size L (Fig. 16). [At much larger values of r, proportional to the system size L, $C(r)$ changes sign, as a result of the particle conservation sum rule $\int C(r)dr=0$]. This happens because subtracting out the quantity ρ^2 from the correlation function is not correct, since the presence of the ACP causes a density inhomogeneity in the medium that cannot be accounted for by subtracting out a constant quantity. To account for the presence of the pattern we consider the correlation function

$$\Gamma(r,\Delta r)=\langle\delta n(r+R(t))\delta n(r+\Delta r+R(t))\rangle, \tag{16}$$

where $R(t)$ is the location of the active site, r is the distance from the active site, and $\delta n(r+R(t))\equiv n(r+R(t))-\rho-\Psi(r)$ is the fluctuation around the average ACP. A reasonable expectation is that the δn's are independent for large separations Δr, i.e.,

$$\Gamma(r,\Delta r)=\langle\delta n(r+R(t))\rangle\langle\delta n(r+R(t)+\Delta r)\rangle\to 0 \tag{17}$$

as $\Delta r\to\infty$. Now consider averaging the function $\Gamma(r,\Delta r)$ over r. On performing a space average over the right-hand side of Eq. (16), we note that

$$\{\langle\delta n(r+R(t))\delta n(r+\Delta r+R(t))\rangle\}=\{\langle\delta n(r)\delta n(r+\Delta r)\rangle\}. \tag{18}$$

Thus this implies that $\{\langle n(r)n(r+\Delta r)\rangle\}-\{(\rho+\Psi(r))(\rho+\Psi(r+\Delta r))\}$ approaches zero as $\Delta r\to\infty$. This predicts the saturation value of the correlation function

$$C^{\rm sat}=\{(\rho+\Psi(r))(\rho+\Psi(r+\Delta r))\}-\rho^2. \tag{19}$$

To test this, we subtracted this estimate of the saturation value from $C(\Delta r)$ and found that the saturation effect is in fact suppressed strongly (Fig. 16), supporting our interpretation. It is possible that another slightly different definition of the pattern would eliminate the slight shoulder, which remains in Fig. 16, after subtraction of $C^{\rm sat}$.

Usually, if the two-point correlation function saturates as the separation between the two points is increased, the saturation value is associated with a nonzero value of the space-fixed average $\langle n(r')\rangle-\rho$. The unusual aspect here is that there is saturation even though $\langle n(r')\rangle=\rho$.

We studied the manner in which $C(\Delta r)-C^{\rm sat}$ approaches zero as $\Delta r\to\infty$. In the tilted case, we found that the correlation function decays exponentially by studying a model where the rules are the same except that only particles are picked. This corresponds to a case of extreme tilt and is similar to the case studied by [46]. In the untilted case, $C(\Delta r)-C^{\rm sat}$ decays as a power law $\sim r^{-\kappa}$ with $\kappa\simeq 0.6$.

VIII. PATTERNS IN OTHER MODELS

In the extremal bond model of interface depinning, we have described the activity-centered pattern in height gradients, which forms as a result of correlated motion of the active site. However, this is not the only sort of pattern that is formed. There is pattern formation also in the value of the average random number f at a site, as a function of the distance from the active site. In analogy with Eq. (2), we define this pattern in random numbers as

$$\Psi_f(r)=\langle f(r+R(t))\rangle-\{\langle f\rangle\}. \tag{20}$$

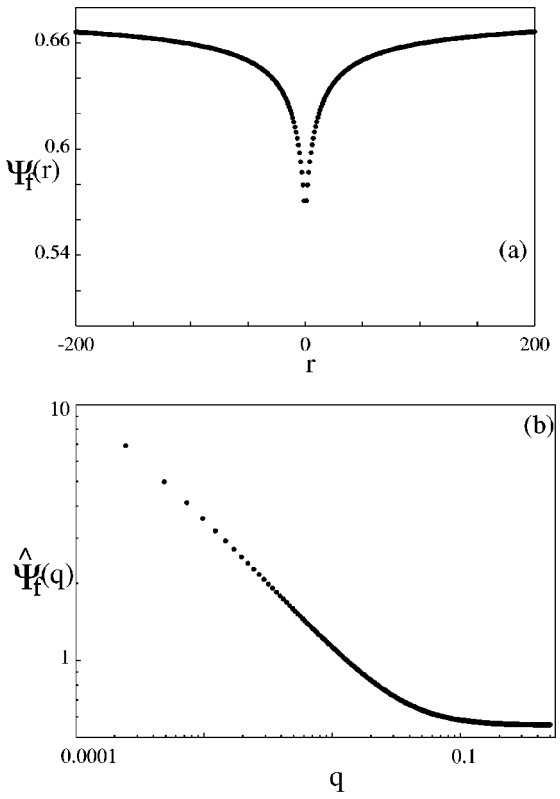

FIG. 17. The pattern in random numbers for the EBM (the untilted case) in (a) real space (b) Fourier space. The Fourier transformed function appears to diverge as a power $q^{-\phi}$ with $\phi \simeq 0.49$ implying a power-law decay $\sim r^{-(1-\phi)}$ at large r for the function in real space. The above data are for a system of size $L=8192$, averaging over 10^7 configurations.

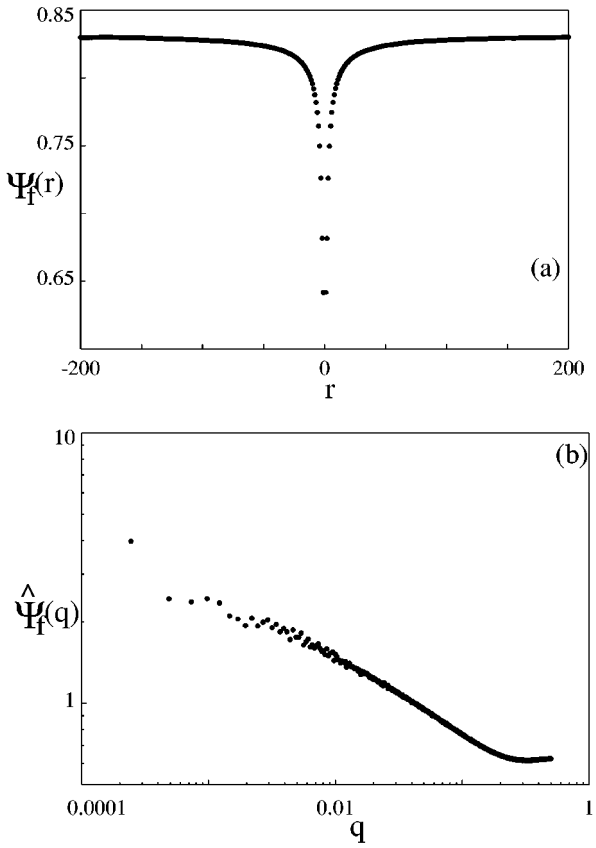

FIG. 18. The pattern in random numbers for the Bak-Sneppen model for evolution in (a) real space (b) Fourier space. The Fourier transformed function appears to diverge as a power $q^{-\phi}$ with $\phi \simeq 0.24$ implying a decay exponent $(1-\phi)$ for the function in real space. This pattern could signify, for instance, the average fitness of a species as a function of the distance from the currently mutating one. The above data are for a system of size $L=8192$ and 10^7 configurations have been averaged over.

Here $f(r+R(t))$ is the random number at a distance r from the active site and the time average $\langle \cdots \rangle$ and space average $\{\cdots\}$ are performed over configurations in the steady state, as before.

Moreover, patterns are found in other extremal models as well. Figures 17, 18, and 19 show the f patterns in the EBM, the Bak-Sneppen model of biological evolution [38], and the Zaitsev model of low-temperature creep [37], respectively. Numerically, it is difficult to directly extract the manner in which the patterns shown in Figs. 17–19 approach their asymptotic values, as fits to power-law decays are very sensitive to the assumed saturation value. We avoided this problem by studying the Fourier transforms of the functions, as the saturation value influences only the single Fourier mode at $q=0$. In all three cases, the Fourier transforms show evidence of power-law behavior as $q \to 0$, implying power-law approaches of the f patterns to their respective saturation values in real space. However, we have not developed an analytical description of the f patterns in any of these models.

Pattern formation thus seems to be generic to extremal models. However, there are instances when considerations of symmetry rule out the formation of a pattern. This is exemplified in the following model, similar in spirit to that considered in [50]. The rules of the dynamics are the same as in the EBM, random numbers are assigned to every site and the minimum is picked, except that there is no net current of particles as there was in the EBM. If the site picked is occupied by a particle, the particle exchanges place with the first hole to its left, and if the site is occupied by a hole, the hole also exchanges place with the first particle to its left. At half filling, there is no net current. This model is the most symmetric of those considered so far and there is no density pattern formed. However, as in the Bak-Sneppen and the Zaitsev models, there is a nontrivial pattern in random numbers in this model.

We emphasize that the feature of the dynamics that is responsible for activity-centered pattern formation is the existence of correlations in the motion of the active site. Extremal models constitute just one class in which there are such correlations. An example of another such class is models of certain types of reaction-diffusion systems, where the activity is quite constrained and correlated. In another physical context, it would seem that coherent structures that form in turbulent flows [51] may well be described by activity-centered patterns. In our definition of the pattern, we take an average over all times, keeping track of the moving structure. This is to be contrasted with previously used methods to identify such moving structures, based on the notion of conditional sampling, namely, averaging only over those time zones in which the activity is at a particular space-time location [51]. Our definition takes configurations at all times

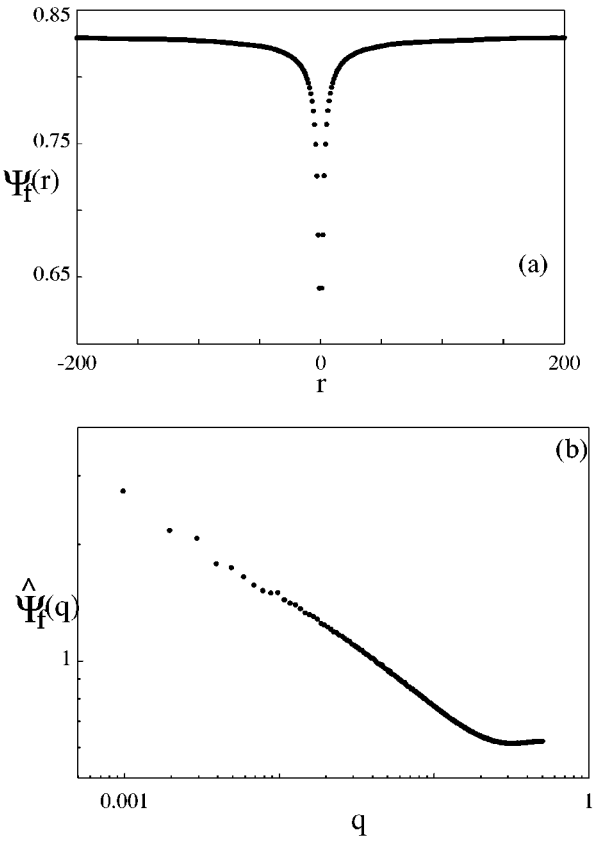

FIG. 19. The pattern in random numbers for the Zaitsev model in (a) real space (b) Fourier space. The Fourier transformed function appears to diverge as a power $q^{-\phi}$ with $\phi \simeq 0.26$ implying a decay $(1-\phi)$ for the function in real space. The data shown are for a system of size $L=2048$, with an average over 10^7 configurations.

into account, but requires a shift of the origin at every instant.

IX. SUMMARY AND CONCLUDING REMARKS

We have introduced a variant of the Sneppen model of interface depinning — the extremal bond model — and have studied the effect of the dynamics of the growth process on the shape of the interface. Our principal result is the observation that there is a nontrivial structure that forms in the interface, and that moves along with the active site. A simple time average of the height gradients, measured in a frame of reference that moves with the active site, defines the activity-centered pattern that serves to quantify the structure. Our numerical study shows that the pattern has a tail that decays as a power law at large distances.

An understanding of the mechanism underlying activity-centered pattern formation was obtained by writing an integral equation that relates the pattern to the probability distribution of active-site jump lengths. The integral equation could be derived by writing an extended master equation for the Lévy-flight model, making it clear that the equation is exact only when there are no temporal correlations between successive jump lengths. In the extremal bond model, however, such correlations are strong. We have shown that a correct description of the pattern, involving temporal correlations, necessitates keeping an infinite hierarchy of equations. Terminating this hierarchy at the very first step results in our integral equation. It would be of interest to understand how much one can better this description by keeping more steps in the hierarchy.

The activity-centered pattern is a one-point function, and so enters the definition of two-point correlation functions. The physical point is that the density inhomogeneity caused by the pattern must be taken into account, by subtracting the relevant quantity from the density-density correlation function. If this is not done, and the square of the nominal density ρ is subtracted instead, the correlation function can exhibit a rather unusual sort of finite size effect. This is an interesting point since the space-fixed time-averaged density at a site is ρ, and it is only the density as defined in Eq. (2) with respect to the moving active site that is different from the nominal density. Yet the space-fixed two-point function is affected by this ''hidden'' pattern.

The presence of the pattern clearly points to a nonhomogeneity in the interface: the region around the active site looks very different on average from the region far away from it. For instance, we expect there to be a larger length of interface in a region of fixed size x around the active site than in a region opposite it. We monitored mean squared fluctuations of the height around the instantaneous average in regions around and opposite the active site, and found a pronounced difference (factor $\simeq 2$, for both tilted and untilted interfaces with $x=256$, $L=4096$). This effect is smaller at stoppers, in keeping with our finding that the pattern itself is suppressed there. This excess length of interface associated with the activity-centered pattern may provide a useful way to identify the active region in experiment.

Finally, it was pointed out that activity-centered pattern formation may occur in a wide variety of other physical contexts, ranging from low-temperature creep of dislocations to structures in turbulent flows. We have presented numerical evidence for this sort of pattern formation in a number of other extremal models. But more generally we expect activity-centered patterns to form whenever there are strong correlations between successive locations of the active site.

ACKNOWLEDGMENTS

We acknowledge helpful discussions with J. K. Bhattacharjee, D. Dhar, G. I. Menon, and M. K. Verma. We are grateful to Goutam Tripathy for help with several of the figures.

[1] J. P. Stokes, A. P. Kushnick, and M. O. Robbins, Phys. Rev. Lett. **60**, 1386 (1988).

[2] M. A. Rubio, C. A. Edwards, A. Dougherty, and J. P. Gollub, Phys. Rev. Lett. **63**, 1685 (1989).

[3] V. K. Horvath, F. Family, and T. Vicsek, J. Phys. A **24**, L25 (1991).

[4] S. He, G. L. M. K. S. Kahanda, and P. Wong, Phys. Rev. Lett. **69**, 3731 (1992).

[5] S. V. Buldyrev, A.-L. Barabasi, F. Caserta, S. Havlin, H. E. Stanley, and T. Vicsek, Phys. Rev. A **45**, R8313 (1992).
[6] J. Zhang, Y.-C. Zhang, P. Alstrom, and M. T. Levinsen, Physica A **189**, 383 (1992).
[7] S. Krishnamurthy and M. Barma, Phys. Rev. Lett. **76**, 423 (1996).
[8] M. Kardar, G. Parisi, and Y.-C. Zhang, Phys. Rev. Lett. **56**, 889 (1986).
[9] D. S. Fisher, in *Nonlinearity in Condensed Matter*, edited by A. R. Bishop, D. K. Campbell, P. Kumar, and S. E. Trullinger (Springer, Berlin, 1987), p. 339.
[10] T. Halpin-Healy and Y.-C. Zhang, Phys. Rep. **254**, 215 (1995).
[11] R. Bruinsma and G. Aeppli, Phys. Rev. Lett. **52**, 1547 (1984).
[12] J. Koplik and H. Levine, Phys. Rev. B **32**, 280 (1985).
[13] D. A. Kessler, H. Levine, and Y. Tu, Phys. Rev. A **43**, 4551 (1991).
[14] G. Parisi, Europhys. Lett. **17**, 673 (1992).
[15] T. Nattermann *et al.*, J. Phys. II **2**, 1483 (1992).
[16] O. Narayan and D. S. Fisher, Phys. Rev. B **48**, 7030 (1993).
[17] Y. -C. Zhang, J. Phys. (France) **51**, 2129 (1990).
[18] J. G. Amar and F. Family, J. Phys. A **24**, L79 (1991).
[19] E. Medina, T. Hwa, M. Kardar, and Y.-C. Zhang, Phys. Rev. A **39**, 3053 (1989).
[20] P. Meakin and R. Jullien, Europhys. Lett. **9**, 71 (1989).
[21] J. G. Amar, P.-M. Lam, and F. Family, Phys. Rev. A **43**, 4548 (1991).
[22] M. H. Jensen and I. Procaccia, J. Phys. II **1**, 1139 (1991).
[23] L. -H. Tang and H. Leschhorn, Phys. Rev. A **45**, R8309 (1992).
[24] K. Sneppen, Phys. Rev. Lett. **69**, 3539 (1992).
[25] L. -H. Tang and H. Leschhorn, Phys. Rev. Lett. **70**, 3832 (1993).
[26] N. Martys, M. Cieplak, and M. O. Robbins, Phys. Rev. Lett. **66**, 1058 (1991); N. Martys, M. O. Robbins, and M. Cieplak, Phys. Rev. B **44**, 12 294 (1991).
[27] R. Lenormand and S. Bories, C. R. Seances Acad. Sci., Ser. B **291**, 279 (1980).
[28] R. Chandler, J. Koplik, K. Lerman, and J. F. Willemsen, J. Fluid Mech. **119**, 249 (1982).
[29] D. Wilkinson and J. Willemsen, J. Phys. A **16**, 3365 (1983).
[30] R. Lenormand and C. Zarcone, Phys. Rev. Lett. **54**, 2226 (1985); see M. Sahimi, Rev. Mod. Phys. **65**, 1393 (1993) for an account of related experiments.
[31] L. Furuberg, J. Feder, A. Aharony, and T. Jossang, Phys. Rev. Lett. **61**, 2117 (1988).
[32] S. Roux and E. Guyon, J. Phys. A **22**, 3693 (1989).
[33] S. Roux and A. Hansen, J. Phys. I **4**, 515 (1994).
[34] K. Sneppen and M. H. Jensen, Phys. Rev. Lett. **71**, 101 (1993).
[35] H. Leschhorn and L.-H. Tang, Phys. Rev. E **49**, 1238 (1994).
[36] S. Maslov, M. Paczuski, and P. Bak, Phys. Rev. Lett. **73**, 2162 (1994); M. Paczuski, S. Maslov, and P. Bak, Phys. Rev. E **53**, 414 (1996).
[37] S. I. Zaitsev, Physica A **189**, 411 (1992).
[38] P. Bak and K. Sneppen, Phys. Rev. Lett. **71**, 4083 (1993).
[39] J. M. Kim and J. M. Kosterlitz, Phys. Rev. Lett. **62**, 2289 (1989).
[40] P. B. Thomas and M. Paczuski, e-print cond-mat/9602023.
[41] M. Barma, J. Phys. A **25**, L693 (1992).
[42] B. Derrida, J. Lebowitz, E. R. Speer, and H. Spohn, J. Phys. A **24**, 4805 (1991).
[43] D. Dhar, M. Barma, and M. K. Phani, Phys. Rev. Lett. **47**, 1238 (1981).
[44] W. Kinzel, in *Percolation Structures and Processes*, edited by G. Deutscher, R. Zallen, and J. Adler (Hilger, Bristol, 1983), p. 425.
[45] Z. Olami, I. Procaccia, and R. Zeitak, Phys. Rev. E **49**, 1232 (1994).
[46] S. Maslov and Y.-C. Zhang, Phys. Rev. Lett. **75**, 1550 (1995).
[47] L.-H. Tang, M. Kardar, and D. Dhar, Phys. Rev. Lett. **74**, 920 (1995).
[48] S. Maslov, Phys. Rev. Lett. **74**, 562 (1995).
[49] P.-M. Binder, M. Paczuski, and M. Barma, Phys. Rev. E **49**, 1174 (1994).
[50] K. Sneppen and M. H. Jensen, Phys. Rev. E **49**, 919 (1994).
[51] W. D. Mc Comb, *The Physics of Fluid Turbulence* (Clarendon Press, Oxford, 1990).